Observation of 4- and 6-Magnon Bound States in the Spin-Anisotropic Frustrated Antiferromagnet FeI_2

Anaëlle Legros,[1,*] Shang-Shun Zhang,[2,*] Xiaojian Bai,[3,4] Hao Zhang,[2,5] Zhiling Dun,[3] W. Adam Phelan,[6] Cristian D. Batista,[2] Martin Mourigal,[3] and N. P. Armitage[1,†]

[1]*The Institute for Quantum Matter and the Department of Physics and Astronomy, The Johns Hopkins University, Baltimore, Maryland 21218, USA*

[2]*Department of Physics and Astronomy, University of Tennessee, Knoxville, Tennessee 37996, USA*

[3]*School of Physics, Georgia Institute of Technology, Atlanta, Georgia 30332, USA*

[4]*Neutron Scattering Division, Oak Ridge National Laboratory, Oak Ridge, Tennessee 37831, USA*

[5]*Materials Science and Technology Division, Oak Ridge National Laboratory, Oak Ridge, Tennessee 37831, USA*

[6]*PARADIM, Department of Chemistry, The Johns Hopkins University, Baltimore, Maryland 21218, USA*

(Received 15 December 2020; accepted 12 November 2021; published 20 December 2021)

We observe a wealth of multimagnon bound states in the strongly anisotropic spin-1 triangular antiferromagnet FeI_2 using time-domain terahertz spectroscopy. These unconventional excitations can arise in ordered magnets due to attractive magnon-magnon interactions and alter their properties. We analyze the energy-magnetic field spectrum via an exact diagonalization method for a dilute gas of interacting magnons and detect up to 4- and 6-magnon bound states, hybridized with single magnons. This zoo of tunable interacting quasiparticles provides a unique platform to study decay and renormalization, reminiscent of the few-body problems found in cold-atom, nuclear, and particle physics.

DOI: 10.1103/PhysRevLett.127.267201

Insulating spin systems are widely studied for their unconventional ground states, exotic magnetic excitations, and spin textures. Geometrically frustrated lattices, like the 2D antiferromagnetic triangular lattice, can suppress magnetic order at low temperatures and support fractionalized excitations [1,2]. But even a long-range ordered magnet can exhibit excitations different than conventional magnons. For instance, depending on spin-space anisotropies and the range of magnetic interactions, single-magnon quasiparticles can interact attractively with each other, generating multimagnon bound states (BS). The existence of such BS was first predicted in the 1930s by Bethe [3] in 1D quantum magnets, using a spin-1/2 Heisenberg model. These exchange-driven BS are usually observed in 1D ferromagnetic spin chains with $S \leq 1$ [4–6]: two magnons in such a system can bind on adjacent sites because the proximity of two spin flips reduces the energy via the ferromagnetic exchange interaction. Although two-magnon BS have been detected in experiments, evidence for higher-order magnon BS remains scarce. Recently, a 3-magnon BS was observed in a quasi-1D $S = 2$ antiferromagnetic spin chain system [7]. Because of their potential for a deeper understanding of fundamental phenomena in magnetism and of few-body problems, such as the study of quasiparticle renormalization and decay, these excitations are of intense current interest [8–15]. But they are also important for potential technological applications since they can strongly affect the transport properties in a 1D chain of qubits [16].

Here, we study multimagnon BS excitations in the spin-anisotropic triangular lattice antiferromagnet FeI_2. The magnetic Fe^{2+} ions carry $S = 1$ and are distributed on triangular planes [Fig. 1], stacked along the $\boldsymbol{c}$ axis. In zero magnetic field, FeI_2 orders spontaneously in a striped antiferromagnetic phase below $T_N \approx 9$ K [17]. One distinctive feature for the $S = 1$ spins in FeI_2 is that the energy of two spin deviations on a single site—a particular form of 2-magnon excitation called single-ion bound state [SIBS, Fig. 1(d)]—is comparable or even lower than the energy of a single magnon [Fig. 1(c)]: a magnetic excitation with a quantum number $|\Delta S^z| = 2$ would, instead of flipping two different spins from $S^z = +1$ (or -1) to $S^z = 0$, flip only one site from $+1$ (or -1) to -1 (or $+1$). This particular BS with $|\Delta S^z| > 1$ on a single site can be observed because $S > 1/2$. Recent neutron scattering experiments in zero magnetic field at $T < T_N$ revealed that this effect stems primarily from the balance between strong easy axis single-ion anisotropy D and nearest-neighbor ferromagnetic exchange interaction J_1 (with $|J_1/D| \sim 0.1$) [18], although competing further-neighbor exchange interactions are necessary to explain the complex magnetic structure and details of the excitation spectrum. Modeling of the neutron scattering evinced that the large spectral weight and weak dispersion of the SIBS originates from a hybridization with the single-magnon band through off-diagonal exchange interactions. The propensity of FeI_2 to generate multimagnon BS of higher order based on these particular features motivated the thorough study of its magnetic

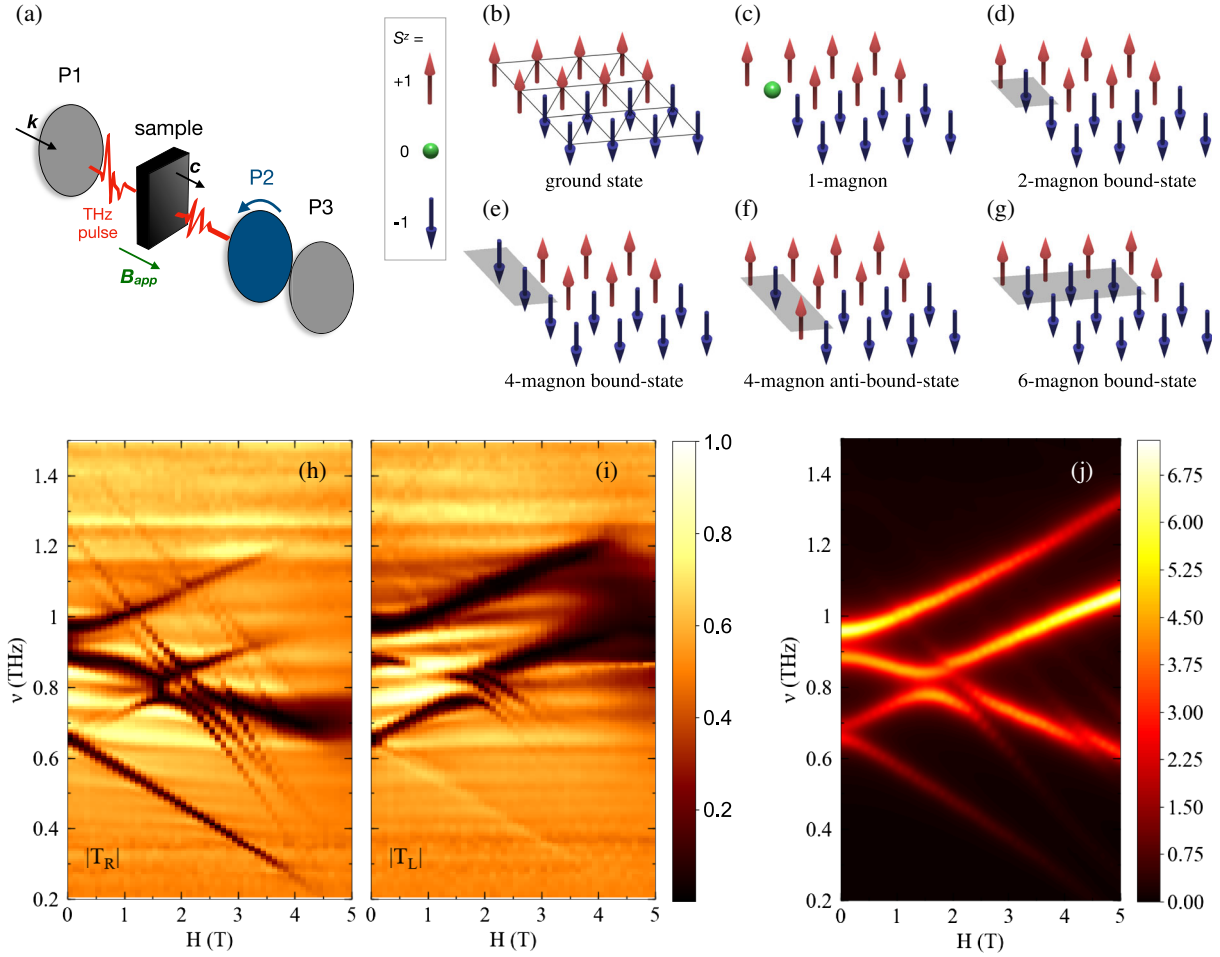

FIG. 1. (a) Sketch of the experimental time-domain terahertz spectroscopy setup [19]: a polarizer ($P1$) linearly polarizes a terahertz waveform that is transmitted through the sample; the sample induces ellipticity; the fast rotating polarizer $P2$ modulates the polarization; a second fixed polarizer ($P3$) projects the rotated light back to the polarization axis defined by $P1$. A dc magnetic field is applied along the sample's $\boldsymbol{c}$ axis in the Faraday geometry (parallel to the THz propagation). (b),(g) Single-ion states of Fe^{2+} ions accessible at low energy correspond to $S = 1$ magnetic moments with uniaxial anisotropy. The sketches represent a plane of spins in the (b) ground state configuration, and examples of (c) a one-magnon elementary excitation (spin wave), (d) a two-magnon bound state (SIBS), (e) a 4-magnon bound state, (f) a 4-magnon antibound state, and (g) a 6-magnon bound state. The gray shadows represent the particular spins that are deviated as compared to the ground state. (h),(i) Magnitude of the transmission coefficients for (h) right- and (i) left-handed circularly polarized lights (normalized to 1), at $T = 4$ K, as a function of frequency and magnetic field (horizontal striations are experimental artifacts). (j) Calculated $\omega[\chi''_{xx}(q = 0, \omega) + \chi''_{yy}(q = 0, \omega)]$ as a function of energy (or associated frequency) and magnetic field, using the exact diagonalization Lanczos method and the model parameters described in the Supplemental Material [20].

excitations. Indeed, as we will see below, the almost flat band nature of the SIBS promotes further BS formation and allows for a rich phenomenology.

FeI_2 undergoes several metamagnetic transitions induced by a $\boldsymbol{c}$-axis magnetic field [21]. Here, we study the low-field antiferromagnetic phase at $T = 4$ K and $\mu_0 H < 5$ T using time-domain THz spectroscopy (TDTS). We observe various low-energy multimagnon excitations (up to 6-magnon character), along with the effects of interactions and hybridization between them. Through a comparison with exact diagonalization calculations for a generalized spin-wave Hamiltonian, our work elucidates how hybridization and interactions between magnetic excitations with different quantum numbers stabilize a low-energy subspace with at least four distinct types of quasiparticles. The presence of distinct low-energy excitations that can be tuned by magnetic field is of general interest for the comprehensive understanding of interacting quasiparticles in materials.

We conducted TDTS measurements as a function of magnetic field ($\mu_0 H \leq 5$ T along the crystal $\boldsymbol{c}$ axis) to study the low-energy magnetic excitations of FeI_2 ($\nu \leq 1.5$ THz $\equiv 6.2$ meV) in the antiferromagnetic phase at $T = 4$ K. TDTS measures the $q = 0$ susceptibility in magnetic insulators. The Faraday geometry of the experiment [Fig. 1(a)] allows us to extract the transmission

eigenstates for both left-handed (LCP) and right-handed circular polarization (RCP) via the polarization modulation technique [19,20,22]. Long time scans of 50 ps associated with reference spectra at higher temperatures [23] yields a high-frequency resolution appropriate for distinguishing resonance peaks separated by $\Delta\nu \approx 0.02$ THz (0.08 meV). While this procedure allows us to measure fine features in the spectra, it prevents us to extract the magnitude of the transmission coefficients with quantitative precision. We thus normalize intensity plots to their maximum value. The frequency (ν) and magnetic field ($\mu_0 H$) dependence of the complex transmission functions, plotted in magnitude as $|T_R|$ [RCP, Fig. 1(h)] and $|T_L|$ [LCP, Fig. 1(i)] shows dark regions corresponding to strong absorption. We associate these absorptions with a wealth of distinct magnetic excitations with crossings and hybridizations. At fixed frequency and field, most branches show a different response in the RCP and LCP channels; several resonances appear in both channels. The steep slope of several branches is clear evidence for their multimagnon character, as discussed further below. Earlier far-infrared spectroscopy and electron spin resonance studies [24,25] observed the zero-field absorption branches at $\nu = 0.65$, 0.88, and 0.97 THz. The high energy and field resolution of our experiments uncover new and very steep branches, as well as additional details that are important to fully understand the low-energy excitations of FeI_2 [see Supplemental Material (SM) [20] for comparison to earlier results].

To gain further insight, we extract the absorption lines' position by inspecting the spectra for both polarization channels [Fig. 2(a)]. Weak modes are sometimes difficult to track from these spectra, and we infer their energies from 2D intensity plots, along with error-bar estimates. Figure 2(a) elucidates the slope of all branches, i.e., the different $\boldsymbol{c}$-axis magnetization S^z of the underlying excitations, but also crossings and hybridizations between modes with different slopes. Given that the uniform magnetization is small below 5 T, these excitations can be further characterized via the sign of S^z relative to the magnetic field. In Faraday geometry, this is related to circular dichroism, given by the imaginary part of the complex angle $\theta_F = \arctan[(T_R - T_L)/i(T_R + T_L)]$, the ellipticity [20], as a function of frequency and magnetic field [Fig. 2(b)]. As absorptions mainly appear in either the RCP or LCP channel, this accentuates the fact that different excitation branches exhibit different signs of S^z [Fig. 2(b)].

The field dependence of the excitation energies yields effective g factors, from which we identify at least four kinds of excitations, including the previously reported single-magnon and 2-magnon excitations [branches no. 1 to no. 4 in Fig. 2(a)], the latter with SIBS character [Figs. 1(c) and 1(d)]. Because the SIBS have an almost flat dispersion throughout the Brillouin zone [18], and given the ferromagnetic nature of nearest-neighbor exchange interactions, SIBS display a strong propensity to form BS with themselves. Therefore, we infer that excitations with the highest effective g factors [branches no. 5 to no. 9 in Fig. 2(a)] are BS comprising primarily two and three SIBS, i.e., 4-magnon [Fig. 1(e)] and 6-magnon BS [Fig. 1(g)], respectively. The tendency of FeI_2 to generate low-energy excitations made of magnon pairs (2, 4, and 6 magnons) can be understood by the effective spin $S = 1$ associated to a large single-ion anisotropy ($|J_1/D| \sim 0.1$): since FeI_2 is a uniaxial system, it is energetically favorable for spins to be in a $S^z = +1$ (or -1) state rather than $S^z = 0$, so spin deviations will concentrate on single lattice sites. For these excitations, the extracted effective g factors do not reach precisely the maximum hypothetical values of twice, four times, or six times that of single magnon excitations. This arises via the

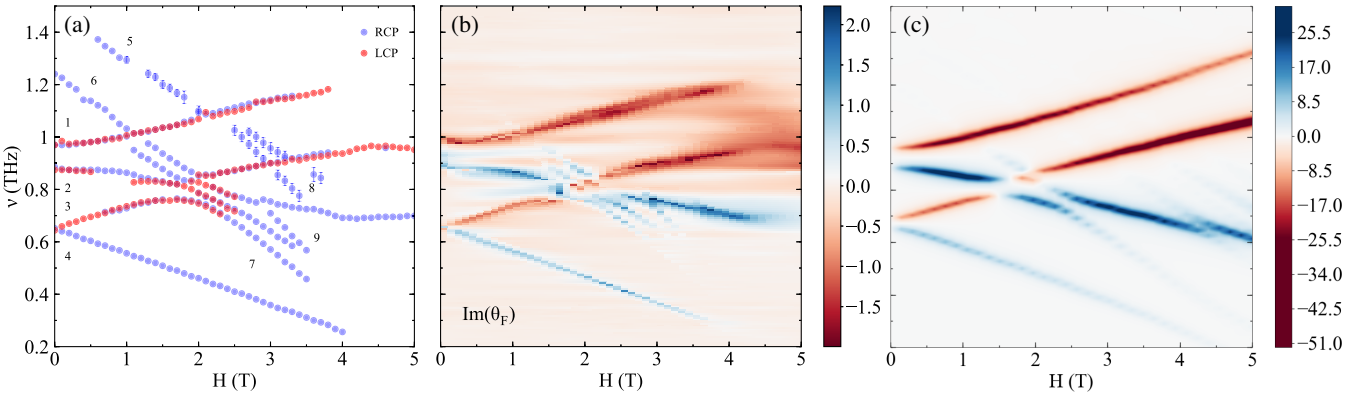

FIG. 2. (a) Position of the magnetic resonances at $T = 4$ K as a function of frequency and magnetic field. All resonances in both circular channels are represented (with some overlap) and correspond to dips in the transmission spectra, except for the data points with error bars which are only distinguishable in the 2D color plot of Fig. 1(h) and assigned by eye. We use numbers to label the different excitation branches (see SM for extracted values of g factors). (b) Imaginary part of the complex Faraday angle θ_F (ellipticity) in arbitrary units, at $T = 4$ K, as a function of frequency and magnetic field. (c) Calculated $\omega[\chi''_{+-}(q = 0, \omega) - \chi''_{-+}(q = 0, \omega)]$ as a function of energy (frequency) and magnetic field, using the exact diagonalization method.

hybridization between the different excitations, e.g., a 4-magnon BS can still be regarded as a BS of two SIBS, but other states mix in when proximate in energy. Similar to neutron scattering experiments [18], the multimagnon BS in FeI_2 only become detectable in TDTS due to their hybridization with single-magnon modes.

Additional insight is gained by calculating the absorption spectra using the microscopic spin-exchange Hamiltonian

$$\mathcal{H} = \sum_{\langle ij \rangle} \sum_{\mu\nu} S_i^{\mu} \mathcal{J}_{ij}^{\mu\nu} S_j^{\nu} - \sum_i [D Q_i^{zz} + \mu_0 \mu_B g H S_i^z], \quad (1)$$

where $Q_i^{zz} = (S_i^z)^2 - 2/3$. The values of the exchange parameters $\mathcal{J}_{ij}^{\mu\nu}$ and single-ion anisotropy D have been obtained by adjusting the parameters from the zero-field neutron scattering study [18], to fit the zero-field THz data with the nonlinear generalized spin-wave theory (GSWT) [20]. The g factor, $g = 3.74$, was obtained by fitting the THz data for finite values of the magnetic field. As previously demonstrated, the nearest-neighbor interactions in FeI_2 are spatially anisotropic and include symmetric off-diagonal terms, $J_1^{z\pm}$ and $J_1^{\pm\pm}$, that are responsible for the hybridization between states with different S^z, such as the single-magnon and SIBS. A GSWT Hamiltonian describes the model's low-energy spectrum as a dilute gas of interacting single-magnon and SIBS quasiparticles, which are treated on equal footing [18,26]. To study this problem beyond linear spin-wave theory, we enforce the dilute limit by eliminating states with more than two quasiparticles from the Hilbert space and perform an exact diagonalization (ED) of the restricted spin-wave Hamiltonian on a finite lattice of $5 \times 5 \times 5$ unit cells, i.e., 500 spins (see SM for details about the computational method, which is based on Refs. [27,28]). As the Hilbert space dimension becomes prohibitively large for ED if we include states with three quasiparticles, our calculation can only account for 1-, 2- and 4-magnon excitations and ignores the 6-magnon states.

The results of our calculations are shown through the angular average of the frequency-weighted susceptibility $\omega[\chi''_{xx}(q=0,\omega) + \chi''_{yy}(q=0,\omega)]$ [Fig. 1(j)] and as the difference between the absorption in the right and left channels via $\omega[\chi''_{+-}(q=0,\omega) - \chi''_{-+}(q=0,\omega)]$ [Fig. 2(c)]. Both plots exhibit a remarkable correspondence with the experimental data (excepting the absence of 6-magnon excitations in ED). Compared to the linear GSWT approach of Ref. [18], ED includes nonlinear interactions that slightly renormalize quasiparticle energies. Therefore, precisely reproducing the energies of the low-energy modes in zero field requires us to slightly adjust the parameters in Eq. (1) compared to Ref. [18], as mentioned above.

ED calculations give the absolute value of the change in $\boldsymbol{c}$-axis magnetization $|\Delta S^z|$ for each excitation branch as a function of frequency and magnetic field [Fig. 3]. Since the striped magnetic structure of FeI_2 has several sublattices, we expect various branches to be present for each magnon sector, some of which optically inactive due to sublattice effects (see SM for selection rules details). The color-coded calculated value of $|\Delta S^z|$ shows that without hybridization ($J_1^{z\pm} = J_1^{\pm\pm} = 0$), excitations have a well defined S^z character, with single and two-magnon modes in purple and blue, respectively [Fig. 3(a)]. The four two-magnon branches are degenerate at zero field as SIBS are localized on each lattice site. They are also optically inactive because our spectroscopic probe can only account for transitions with $\Delta S^z = \pm 1$. The Zeeman term splits the zero-field SIBS quartet into two doublets. With hybridization, the two SIBS doublets are split by the $J^{z\pm}$ term via hybridization with *nondegenerate* single-magnon modes [Fig. 3(b)], and the two-magnon branches that hybridize with the two

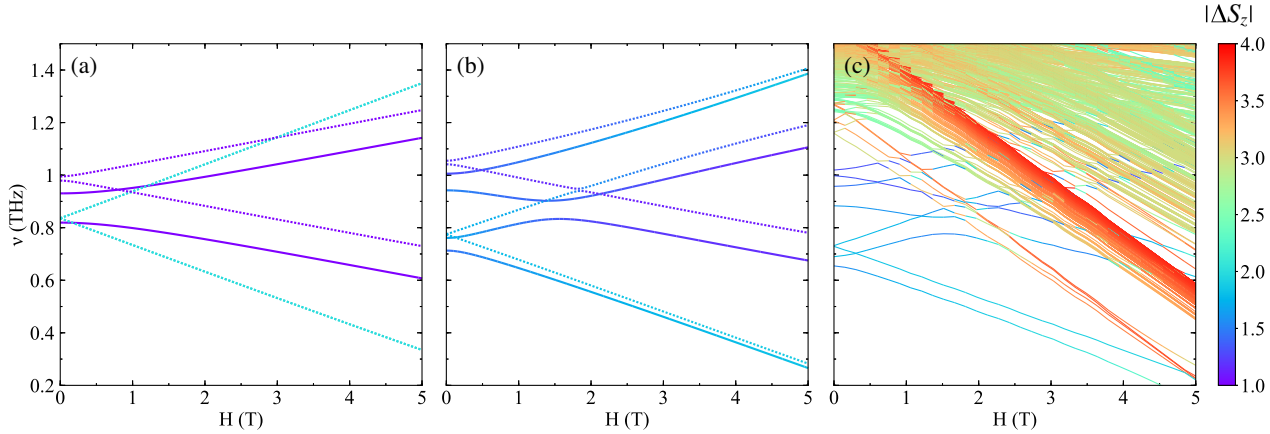

FIG. 3. Calculated $|\Delta S^z|$ using ED of a GSWT Hamiltonian including (a) only single and two-magnon excitations, without hybridization terms ($J_1^{z\pm} = J_1^{\pm\pm} = 0$), where full (dotted) lines correspond to optically active (inactive) branches due to sublattice effects; (b) same as (a) but including hybridization effects; (c) same as (b) but with the addition of 4-magnon BS and no distinction between optically active and inactive branches. These plots give an insight into the character of the various magnetic excitations and the hybridization between them.

optically active one-magnon branches become detectable. Including 4-magnon excitations yields a rich excitation spectrum with several hybridization effects between all types of excitations between 1 and 4 T [Fig. 3(c)].

These results highlight that the character of magnetic excitations in FeI_2 in an applied magnetic field is profoundly affected by their strong mutual hybridization; most branches have a mixed and changing $|\Delta S^z|$ character. Therefore, even if the effective g factors give some insight into the nature and degeneracies of the observed resonances, labeling excitations based on their S^z is not possible. Given that excitation branches no. 5, no. 6, and no. 7 from Fig. 2(a) have primarily 4-magnon character by comparison to theoretical predictions [Fig. 3(c)], the larger slope of branches no. 8 and no. 9 indicate an even higher-order character, i.e., these are primarily 6-magnon BS. The hybridization of 4- and 6-magnon BS with lower-order excitations has three important consequences: they become detectable in TDTS in the proximity of energy crossings; it explains why the effective g factors of the steeper branches do not reach their hypothetical maximum values, as mentioned above; it explains why the four low-field branches [no. 1 to no. 4 in Fig. 2(a)] have comparable absorption and similar slopes (they are roughly equal mixtures of single and two-magnon excitations).

To a large extent, a fundamental quest in modern condensed matter physics is the search for novel emergent quasiparticles and excitations. Our TDTS experiments on FeI_2 unraveled a wealth of multimagnon excitations, including 4- and 6-magnon bound states. Exact diagonalization calculations of a generalized spin-wave Hamiltonian [18] elucidated spectral contributions from each $|\Delta S^z|$ sector, enabling a complete understanding of the microscopic character of excitations up to 4-magnon modes. The strong hybridization that stems from spin-space anisotropy leads to a unique spectroscopic situation where bound states and their interactions can be tracked as a function of magnetic field. Thus, FeI_2 is a promising field-tunable material platform to study fundamental quantum phenomena in magnetism and strongly interacting few-body models encountered in various contexts such as excitons in semiconductors, cold atoms, and nuclear and particle physics.

Work at JHU (A. L, N. P. A.) was supported as part of the Institute for Quantum Matter, an EFRC funded by the DOE BES under DE-SC0019331. A. L. and N. P. A thank Howard Katz and Jinfeng Han from the Department of Materials Science and Engineering at JHU for providing the necessary equipment to prepare the sample for measurements. The work at GT (X. B., Z. L. D., M. M.) and the University of Tennessee (S.-S. Z., H. Z., C. D. B.) was supported by the DOE BES under Award No. DE-SC-0018660. The work by H. Z. was supported by the Graduate Advancement, Training and Education (GATE) program of UTK and ORNL. Growth of FeI_2 crystals is based upon work supported by the National Science Foundation [Platform for the Accelerated Realization, Analysis, and Discovery of Interface Materials (PARADIM)] under Cooperative Agreement No. DMR-1539918.

*These authors contributed equally to this work.
†To whom correspondence should be addressed.
npa@jhu.edu

[1] C. Broholm, R. J. Cava, S. A. Kivelson, D. G. Nocera, M. R. Norman, and T. Senthil, Science **367**, 6475 (2020).
[2] M. J. P. Gingras and P. A. McClarty, Rep. Prog. Phys. **77**, 056501 (2014).
[3] H. Bethe, Z. Phys. **71**, 205 (1931).
[4] J. B. Torrance and M. Tinkham, Phys. Rev. **187**, 595 (1969).
[5] R. Hoogerbeets, A. J. v. Duyneveldt, A. C. Phaff, C. H. W. Swuste, and W. J. M. d. Jonge, J. Phys. C **17**, 2595 (1984).
[6] P. Chauhan, F. Mahmood, H. J. Changlani, S. M. Koohpayeh, and N. P. Armitage, Phys. Rev. Lett. **124**, 037203 (2020).
[7] R. L. Dally, A. J. R. Heng, A. Keselman, M. M. Bordelon, M. B. Stone, L. Balents, and S. D. Wilson, Phys. Rev. Lett. **124**, 197203 (2020).
[8] Y. Nishida, Y. Kato, and C. Batista, Nat. Phys. **9**, 93 (2013).
[9] Y. Kato, S.-S. Zhang, Y. Nishida, and C. D. Batista, Phys. Rev. Research **2**, 033024 (2020).
[10] Z. Wang, J. Wu, W. Yang, A. K. Bera, D. Kamenskyi, A. N. Islam, S. Xu, J. M. Law, B. Lake, C. Wu, and A. Loidl, Nature (London) **554**, 219 (2018).
[11] A. Keselman, L. Balents, and O. A. Starykh, Phys. Rev. Lett. **125**, 187201 (2020).
[12] M. Yoshida, K. Nawa, H. Ishikawa, M. Takigawa, M. Jeong, S. Krämer, M. Horvatić, C. Berthier, K. Matsui, T. Goto, S. Kimura, T. Sasaki, J. Yamaura, H. Yoshida, Y. Okamoto, and Z. Hiroi, Phys. Rev. B **96**, 180413(R) (2017).
[13] S. Pradhan, N. D. Patel, and N. Trivedi, Phys. Rev. B **101**, 180401(R) (2020).
[14] S. Ward, M. Mena, P. Bouillot, C. Kollath, T. Giamarchi, K. P. Schmidt, B. Normand, K. W. Krämer, D. Biner, R. Bewley, T. Guidi, M. Boehm, D. F. McMorrow, and Ch. Rüegg, Phys. Rev. Lett. **118**, 177202 (2017).
[15] D. Wulferding, Y. Choi, S.-H. Do, C. H. Lee, P. Lemmens, C. Faugeras, Y. Gallais, and K.-Y. Choi, Nat. Commun. **11**, 1603 (2020).
[16] V. Subrahmanyam, Phys. Rev. A **69**, 034304 (2004).
[17] A. R. Fert, J. Gelard, and P. Carrara, Solid State Commun. **13**, 1219 (1973).
[18] X. Bai, S.-S. Zhang, Z. Dun, H. Zhang, Q. Huang, H. Zhou, M. B. Stone, A. I. Kolesnikov, F. Ye, C. D. Batista, and M. Mourigal, Nat. Phys. **17**, 467 (2021).
[19] C. M. Morris, R. V. Aguilar, A. V. Stier, and N. P. Armitage, Opt. Express **20**, 12303 (2012).
[20] See Supplemental Material at http://link.aps.org/supplemental/10.1103/PhysRevLett.127.267201 for methods used to grow the crystal, carry out the time-domain terahertz spectroscopy experiments (along with a comparison to older work), as well as details on the generalized spin-wave theory and values of model parameters.

[21] A. Wiedenmann, L. P. Regnault, P. Burlet, J. Rossat-Mignod, O. Koundé, and D. Billerey, J. Magn. Magn. Mater. **74**, 7 (1988).

[22] L. Pan, S. K. Kim, A. Ghosh, C. M. Morris, K. A. Ross, E. Kermarrec, B. D. Gaulin, S. Koohpayeh, O. Tchernyshyov, and N. Armitage, Nat. Commun. **5**, 4970 (2014).

[23] C. M. Morris, R. Valdés Aguilar, A. Ghosh, S. M. Koohpayeh, J. Krizan, R. J. Cava, O. Tchernyshyov, T. M. McQueen, and N. P. Armitage, Phys. Rev. Lett. **112**, 137403 (2014).

[24] D. Petitgrand, A. Brun, and P. Meyer, J. Magn. Magn. Mater. **15**–**18**, 381 (1980).

[25] K. Katsumata, H. Yamaguchi, M. Hagiwara, M. Tokunaga, H.-J. Mikeska, P. Goy, and M. Gross, Phys. Rev. B **61**, 11632 (2000).

[26] R. A. Muniz, Y. Kato, and C. D. Batista, Prog. Theor. Exp. Phys. **2014**, 083I01 (2014).

[27] E. R. Gagliano and C. A. Balseiro, Phys. Rev. Lett. **59**, 2999 (1987).

[28] C. Lanczos, *An Iteration Method for the Solution of the Eigenvalue Problem of Linear Differential and Integral Operators* (United States Government Press Office Los Angeles, CA, 1950).